# Entry Flow Alignment of Wormlike Micelles through an Abrupt Contraction

Viviane Lutz Bueno[1], Joachim Kohlbrecher[2], Peter Fischer[1]

[1] Institute of Food Science and Nutrition, ETH Zurich, 8092 Zurich, Switzerland
[2] Laboratory for Neutron Scattering, PSI, 5232 Villigen PSI, Switzerland

ABSTRACT

Diluted viscoelastic surfactant solutions flowing though contractions form unusual upstream jetting flows. Their structural origin was investigated. Sample degradation was avoided using aluminum-glass flow cells and polyolefin tubing. SANS measurements showed that micellar orientation occurs during extensional flow, depending on the applied rate, position in the channel and spatial confinement.

## INTRODUCTION

The formation of micelles in aqueous solutions of surfactant is entropically favorable, if compared to energy of the same molecules unlinked, since it happens to remove the hydrophobic groups of the surfactant polar head from the contact with water[1]. These aggregates can acquire different shapes and sizes[2]. Worm-like micelles are formed depending on their critical micelle concentrations (CMC, 0.83 mM for pure cetyl trimethylammonium bromide, CTAB[3]). When the concentration is higher than the CMC, long polymeric-like chains are formed; when the concentration is lower, the molecules aggregate into spherical micelles[1]. In even higher concentrations the worm-like micelles grow in length and the solution exhibits viscoelastic properties[2]. Yet, if aromatic additives like salts (like sodium salicylate, NaSal) are added into the system, the CMC of the transition is lowered, so the spherical to worm-like micelle transition happens at lower concentrations, as well as the viscoelastic behavior. It is due to the strongly binding counterions present in the salt composition[3].

The ratio of salt/surfactant is important. Equimolar concentrations (1:1) were chosen for this work, since the number of counterions and the available polar head groups is the same, so they can easily bind, avoiding the effects of ions in excess. When more salt is added, for instance, the counterions are adsorbed not only on the surface of the worm-like micelle, but also penetrate into them, what can cause charged micelles which break down due to the repulsive forces, decreasing in length and also the viscoelastic response[4]. This ratio defines the size, shape and organization of the micelles[2]. So, for equimolar solutions, the formation of wormlike micelles is guaranteed. Also, shear thinning behavior is expected for 1:1 CTAB/NaSal solutions as well as more uniform size distribution[5].

When the concentration is higher than 10 mM, a gel-like behavior is developed due to micellar interaction what complicates the rheological characterization[6]. The micellar microstructure will also depend on the temperature of the system, on the ionic strength of the ions in solution and on the concentration of surfactant[5-7].

Though, under influence of a flow field, the structure of the micelles can be modified, particularly when they are charged and partially or no shielded by the addition salt[7]. These concentrations diminish the Brownian contributions, since long flexible chains are formed what changes the flow properties of these solutions[6]. Studies of the alignment

and orientation of micelles under external flow have been developed intensively[3,8]. The wormlike micellar solutions are known as live polymers since they can break into smaller micelles generating micelles with residual charge and also regenerate[5]. These characteristics lead to the formation of complex structures under flow, demonstrated as shear banding[1,2,8]. If the shear stress is kept constant, the oscillations can become periodic[9,10] and the system does not achieve an equilibrium state[11], showing that the equilibrium phase behavior can be influenced by the flow. For wormlike micelles, the dynamics of the stress relaxation is related to the breaking process[5]. The concentration of 7.5 mM was defined as the limit between the dilute (micrometric linear chains) and semi-dilute solutions (when the chains become to entangle and a three dimensional net-work is formed)[3].

Dilute to semi-dilute surfactant and surfactant/salt solutions which have viscoelastic behavior are well known, since they exhibit flow-induced phase transitions as well as banded flow profiles, which lead to non-linear and transient flow properties[12-15]. These viscoelastic properties together with the behavior under flow are largely employed in many applications, like for instance: drag reduction[2], oil and gas production, smart gels and nanobiotechnology[16].

The highly elastic features of the surfactant system CTAB/NaSal at low concentrations lead to an upstream jetting flow when moving through a planar contraction. These flows are highly influenced by inertia and elasticity[17]. Extensional flows have many applications with non-Newtonian liquids, from polymer processing to ink-jet printing[18]. The measurement of the extensional viscosity is still a challenge and many methods are being developed, for example: hyperbolic contractions[18], confined circular cylinder[8], birefringence[1], soft lithography, streakline photography, particle-image velocimetry[8], small angle neutron scattering and pressure drop measurements[8].

Rodd et al.[17] has shown the effects of a flow through an abrupt contraction followed by an abrupt expansion, using dilute and semi-dilute polymers. The entry flow could be characterized by the contraction ratio ($\beta$), Reynolds number, $Re=\rho V_c D_k/\eta_0$ ($\rho$=density; $V_c$=velocity of the fluid at the contraction entrance; $D_h=2hW_c/(h+W_c)$ = hydraulic diameter of the contraction ($h$ and $W_c$ are the dimensions of the contraction channel); $\eta_0$ = zero-shear rate viscosity) and the Weissenberg number, $W_i=\lambda/T_{flow}$ ($\lambda$=relaxation time of the fluid and $T_{flow}$=characteristic residence time at the contraction region defined by $T_{flow}\approx D_k/V_c$). $Re$ measures the ratio of inertial forces to viscous forces and quantifies the relative importance of these two types of forces for given flow conditions. $Wi$ indicates the degree of anisotropy generated by the deformation. They are also used to define the elasticity number ($El=Wi/Re$), which is the ratio of elasticity and inertia of the fluid.

The flow behavior of 1:1 CTAB/NaSal solutions through a planar 16:2:16 abrupt contraction-expansion geometry was investigated by rheological measurements and by small angle neutron scattering (SANS). Fischer et al.[19] observed that the circulation of CTAB/NaSal solutions in a tubing-pump loop caused the degradation of the sample and becomes impossible the study of the extensional flow. So the life-time of the samples during the SANS measurements was also studied.

## RHEOLOGY OF 1:1 CTAB/ NaSal

Cetyl trimethylammonium bromide (364.45 g/M) and sodium salicylate (160.11 g/M) were obtained from Fluka (Buchs, Switzerland) and used without further purification. Equimolar concentrations of 2.5 and 10 mM CTAB/ NaSal powders were dissolved into 100 ml of Millipore water and mechanically stirred for at least 4 hours. After, the system was maintained still for at least 48 h to recover its transparency.

The rheological analysis was done with a stress-controlled rheometer (Rheometrics Scientific DSR) equipped with a Couette geometry (dimensions: cylinder radii: inner $r_i$ = 14.75 mm, outer $r_o$ = 16.50 mm and height $h$ = 44.40 mm). The temperature was maintained constant (24° C) by a refrigerated/heating circulator (Julabo Labor-Technik F32-HE) connected to the rheometer. Shear stresses between 0.01-20 Pa were applied increasing logarithmic scale. Fig. 1 displays the flow curves of the surfactant/salt solutions of 2.5 and 10 mM.

Cooper-White et al.[3] has shown that when the concentration increases from 0.1 to 10 mM, the micelles undergo from nearly spherical spheres to rod-like to highly extended worm-like chains. The 10 mM solution shear thinned, due to the alignment of the micelles along the flow direction. Also, the disentanglement of the worm-like micelles could have occurred, since the cross-over concentration was visualized around 7.5 mM, where the micelle-micelle interaction starts to be important. Yet, the 2.5 mM solution showed induced shear thickening at low shear rates. The solution was motionless when the stress was applied, so its viscoelastic properties acted as a resistance to start flowing. Shear banding properties and oscillations (due to inertial effects[19]) were also visualized for these low concentration CTAB/ NaSal solutions and were further studied, but are not treated here.

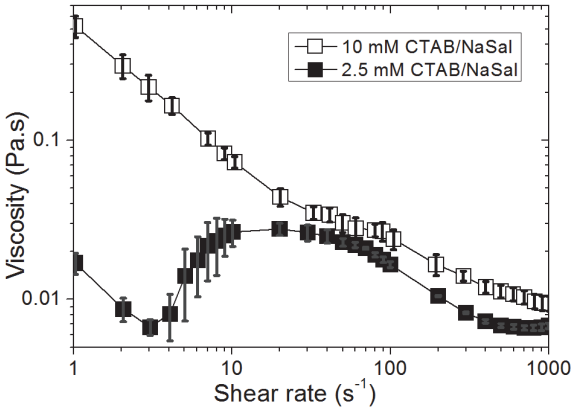


Figure 1. Flow curve of the shear stress from increasing shear stress.

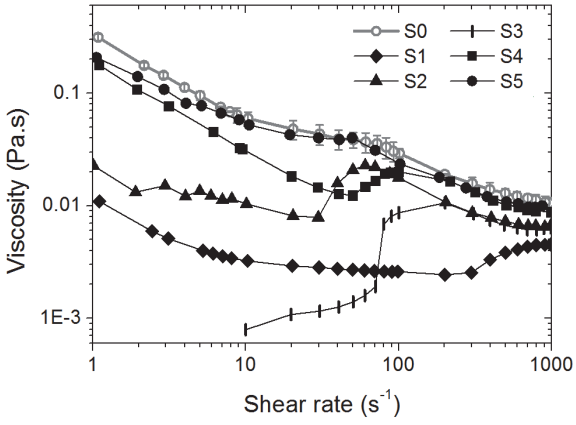


Figure 2. Flow curves after interaction between different polymers and 10 mM CTAB/NaSal solution.

In previous studies, these viscoelastic properties of the CTAB/NaSal solution degenerated within few hours of circulation in the flow cell[19]. Two reasons were considered: mechanical shearing during the flow; and/or solubilization of polymers/ plasticizers in contact with the solution. Equimolar 10 mM CTAB/NaSal was used to study the degradation. The sample was sheared in the Couette geometry under 10 Pa for 10 hours. During this period, no variation of the viscosity was visualized what shows that there is no degradation of the micelles due to shearing.

However, the micellar solutions lost their properties after interacting with thermoplastic polymers. It was determined by measuring their viscosity before and after contact (Fig. 2). The polymeric samples described in Table 1 (Ismatec, Wertheim, Germany) were immersed in 5 ml of 10 mM CTAB/NaSal solution for 48 hours. The weight loss was calculated based on the difference of the polymeric sample mass before and after the immersion, showing that there was a deterioration of the polymer as well.

Table 1 shows between the tubing tested the systems S1 and S2 had the highest weight losses. It could be because of the electronegativity of the halogenic groups

(fluorine and chlorine) which compose those polymers. The polarities of both groups are higher than the one of bromide (CTAB counterion), what leads to a more stable chemical bond. Since the polymer and the surfactant have these similar functional groups, the permeation rate into the polymer could also increase, what starts the diffusion of halogenic groups due to concentration difference. The interaction of the $Cl^-$ with the micelles was less intense for the $Fl^-$, based on the weight loss. The shape of S2 curve resembles the one of lower concentration solutions. Probably, the release of $Cl^-$ ions into the solution broke down some of the wormlike micelles or they disaggregated under reactions between the ions in solution. After that, there were still wormlike micelles in solution, differently from the S1 ($Fl^-$) case.

A high weight loss and viscosity variation was also observed for the S3 system. The composition of the polymer is based on polypropylene (just non-polar groups) and plasticizer which improves the flexibility by spreading the polymeric chains apart, what could have allowed the permeation of the micellar solution. Also, the plasticizer has the tendency to migrate to the surface of the polymer[21] and be leached by the solution, where it could disaggregate the wormlike micelles by chemical reaction driven by the polarity. Comparison between sample S3 and S4 is possible, since both are based on polypropylene. The S4 is modified with elastomer in order to achieve the same properties avoiding the use of plasticizer. From the rheological analysis, it exhibited a lower interaction with the CTAB/NaSal solution, resulting in lower weight loss and viscosity variation[22].

The polyolefin blend tubing (S5) has not changed its physical and chemical properties after contact with the surfactant solution, being stable for long periods. This tubing was used during the SANS experiments and no degradation of the CTAB/NaSal solution was visualized even after long periods of circulation.

Table 1. Tubing material

| Nr. | Name | Tubing composition | Weight loss |
|---|---|---|---|
| S1 | Fluran® HCA | Fluor elastomer | 1.27 % |
| S2 | Tygon® R-3607 | Polyvinylchloride, plasticizer | 0.94 % |
| S3 | Phar Med® | Polypropylene, plasticizer | 0.85 % |
| S4 | Tygon® MHLL | Elastomeric polypropylene | 0.12 % |
| S5 | Tygon® MHSL | Polyolefin blend | 0.01 % |

JETTING FLOW

The experiments were performed at the SANS instrument of PSI, Villigen, Switzerland. The planar contraction geometry was built as an aluminum-glass sandwich, in which the flow was confined. Its dimensions are shown in the Fig. 3. The thickness of the flow cell (y-dimension) was equal to 0.5 or 1.0 mm and the contraction ratio (β) was 8. Fig. 3 also shows the entrance area of the contraction were the SANS images were visualized. The axes of the coordinate system were chosen according to the direction commands of a motion table, on which the flow cell was placed horizontally, allowing further measurements along the x-axis. The scanned area covered a range of z=8 mm and x=40 mm. The set up system was composed of the flow cell, tubes, connectors, tubing pump and cooling system (Fig. 4). The temperature was maintained around 24° C by water circulation along the aluminum frame. The solution was injected in the longer expanded channel in order to achieve a laminar flow at the contraction entrance.

The water in the CTAB/NaSal solutions was replaced with $D_20$ to achieve a better contrast in the scattering patterns of the micelles. The parameters used in the SANS experiments were: flow rates: 0.05-5.00 $cm^3/s$; incident wave length of the neutron

beam: 6 Å; aperture diameter: 1, 2 and 4 mm; detector distance: 2, 6 and 18 m; q-range: 0.03-0.33 $nm^{-1}$.

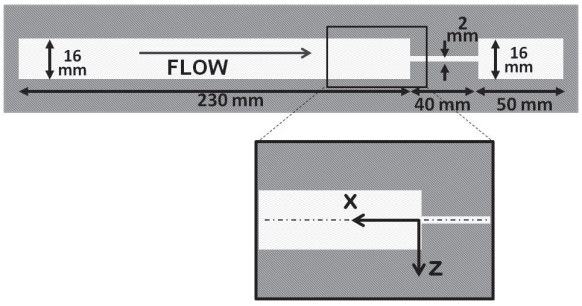


Figure 3. Dimensions of the planar contraction geometry. Detail: SANS scanned area.

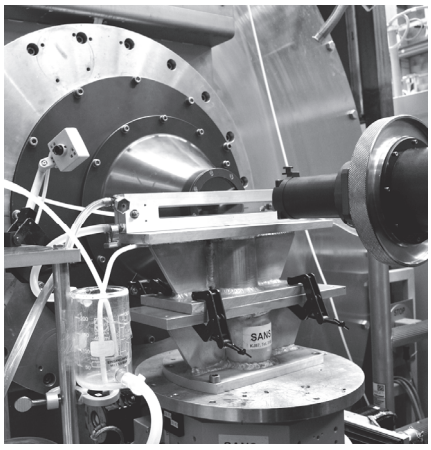

Figure 4. Set up of the SANS experiment with the flow cell and the tubing loop.

The flow rates set on the tubing pump were chosen according to the range of shear rates where just shear thinning happens (higher than 20 1/s on Fig. 1). The flow at the entrance of the contraction channel is symmetric, so just half of the region was scanned. Fig. 5 shows the SANS scattering of the CTAB/NaSal solution at the (4,0) position. The graphical representation takes the 0° as a reference for the radial analysis of the scattering intensity based on the color scale of the pixels. An intensity average was calculated for each 5° arc along the circumference. A sector between the two circles (represented on Fig. 5) was the limit used to avoid pixels with zero contribution. The image analysis was done with GRASP software for SANS data analysis. The resulting graphic is a representation of the 72 average points in function of the azimuthal angle. The curves were normalized to the maximum and used to measure the alignment angle of the micelles, as well as the alignment intensity.

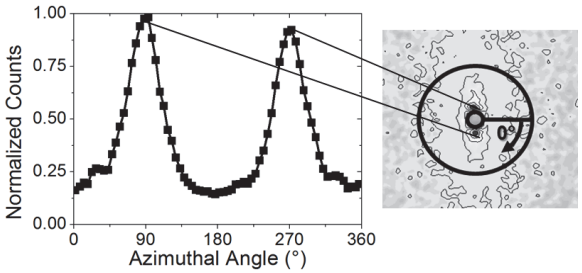


Figure 5. Graphical representation of the SANS scattering patterns.

Another factor calculated based on the SANS analysis, was the anisotropy factor ($A_f$), which is a good representation of the scattering pattern shape reduced into a simple number[23]. It is a correlation between the difference of the sum of the intensities along the vertical ($I(q)_\perp$) and horizontal direction ($I(q)_\parallel$) in function of q (scattering length) of the SANS scatter (Fig. 6a), divided by the vertical scattering, as shown in Eq. 1[24].

$$A_f = \frac{I(q)_\perp - I(q)_\parallel}{I(q)_\perp} \quad (1)$$

The anisotropy factors calculated based on Eq. 1 considered micelles aligned along either the vertical (flow direction) or horizontal (perpendicular to the flow) axis. It is not the case for our study, since at the contraction entrance the micelles have also diagonal alignments, generating scattering patterns which are not aligned along those axes (Fig. 6b, c and d). The Eq. 2 was adjusted to these different alignments, considering the maximum and minimum scattering angles as the main axes. They were set as the center of 60° arcs, which were used to define the areas to sum up the intensities. These angles were selected based on the graphic representation of the scattering pat-

tern image, which varies the peaks position (angle) according to the micelle alignment (Fig.5). Eq. 2 can be used to calculate the anisotropy factor with different micelle orientation. $I(\theta_{max})$ is the sum of the scattered intensities over arcs of 60° centered on the maximum scattering angle and $I(\theta_{min})$ is centered on the minimum scattering angle (Fig. 6b).

$$A_f = \frac{I(\theta_{\max}) - I(\theta_{\min})}{I(\theta_{\max})} \qquad (2)$$

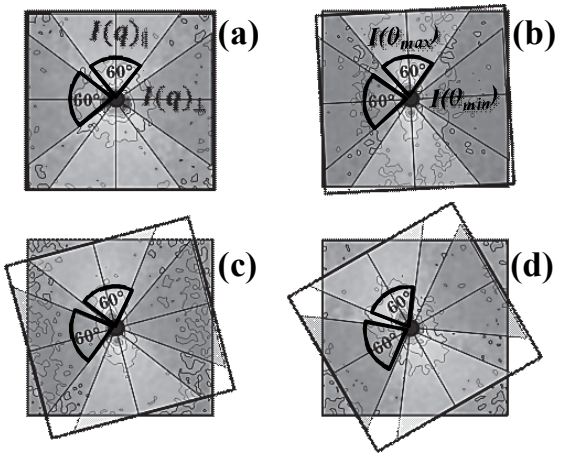


Figure 6. Examples of the directions used for the anisotropy factor calculation.

Fig. 7 shows the graphical representation of the scattering patterns based on 12 images along the (x, z) plane at the contraction entrance of a 2.5 mM CTAB/NaSal solution at 0.09 $cm^3/s$. The measurements started at the contraction entrance (0,0), afterwards the neutron beam was moved to z = 2, 4 and 6. When z=0 (first column on the right in Fig. 7), the three scattering images are aligned nearly parallel to the z-axis (90° and 270° angles), considering that they are located in the centerline of the flow. The alignment is higher closer to the contraction entrance. When z=2 mm, there were alignments along different angles, following a trend to vertical alignment when x position increases. The (0,2) point shows a weak alignment, probably because it is too close to the edge of the flow cell. In z=4 mm, the anisotropy of the alignment decreased. The (0,4) point shows a circular scattering. The points along Z=6 have lower alignment. The point (0,6) shows a nearly isotropic scattering (circular pattern). The points close to the corner of the flow cell probably do not align even under high shears, due to the extensional properties of the fluid.

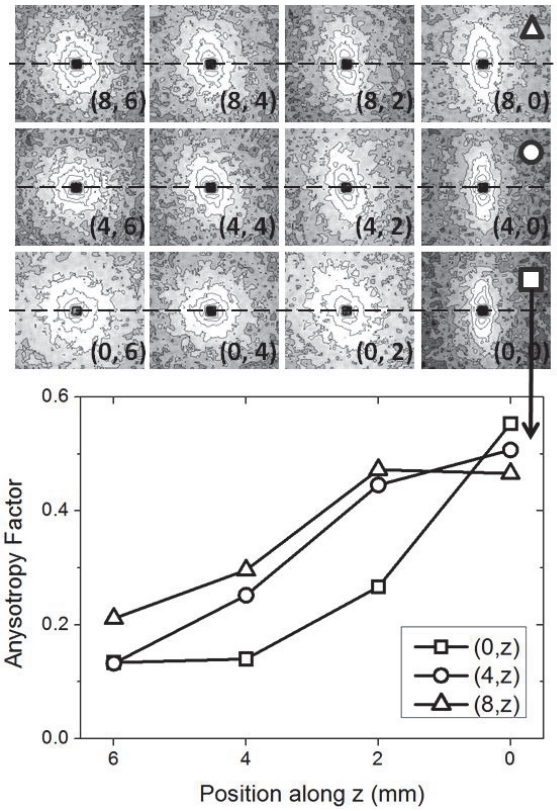


Figure 7. Scattering patterns at different (x, z) positions along the flow cell (y=1mm); Graph: anisotropy factor as a function of upstream position (z).

Fig. 7 also shows the corresponding anisotropy factors in function of different spatial positions in the flow cell. High values of the $A_f$ at the center positions (x,0) indicate the jetting regime (since the micelles are aligned along the flow) and low values at the wall region (x,6) indicate material at rest or under low shear (what generates the spherical pattern or the low alignment with the flow).

The calculation of the *Re* and *Wi* numbers was done. The relaxation times were

based on the measurements by Cooper-White et al[3], but below 7.5 mM the solutions could not be measured due to the lack of transducer torque resolution. So, the relaxation times for dilute CTAB/NaSal solutions have to be further studied. Considering the values obtained for 10 mM ($\lambda$=226 s) the elastic number obtained was $2.58 \times 10^5$. The Fig. 8 shows the Reynolds number calculated for different flow rates and confinements (y-direction). The hollow symbols are related to the 1 mm flow cell and the full ones to the 0.5 mm flow cell. The curves increased the *Re* with the flow rate, what proves the increasing effects of the inertia to the flow. Also, there was a displacement according to the y-dimension and concentration. The higher Reynolds number calculated was for the 2.5 mM CTAB/NaSal solution at y=5 mm, what proves that the confinement increases the inertial effects. In the detail of Fig. 8, the plot of *Re* vs. *Wi* for the 10 mM solution shows comparable results to Rodd et al. for shear thinning fluids[17].

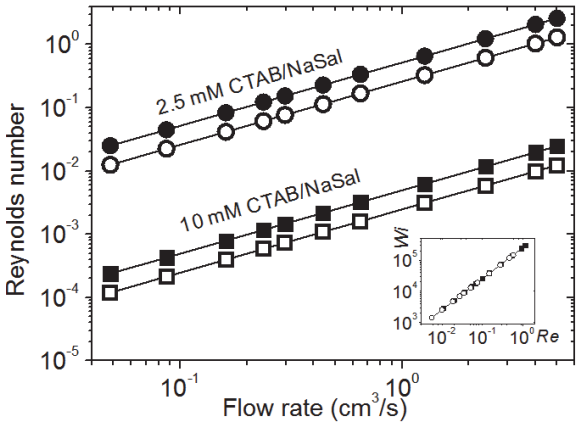


Figure 8. Reynolds number as function of flow rates. Different concentrations and confinements were used (hollow symbols: y=1.0 mm, full symbols: y=0.5 mm).

The influence of confinement, i.e. flow cell thickness (y = 0.5 or 1 mm) on the anisotropy factor is shown in Fig. 9. There, the $A_f$ is plot for different (x, z) positions, which generated different shear rates (x-axis) depending on the flow rate and cell thickness. Due to the reduced cross section of the thinner cell, higher flow rates could be achieved. Also, high alignment (increase of the anisotropy values) is seen in the filled symbols the center position (4, 0) to (40, 0). For the filled symbols all shear rates are higher than 150 1/s. This indicates that the micellar alignment was achieved through the entire flow cell. The existence of a jetting flow along the centerline of the flow cell was proved and quiescent flow towards the cell boundaries and can propose a confinement-free scaling of the $A_f$.

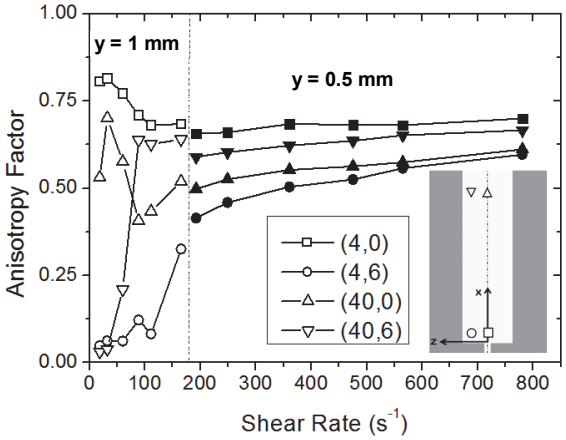


Figure 9. Anisotropy factor for different flow rates and (x, z) positions under different y-confinement.

## CONCLUSION

The formation of the jetting flow could be verified by SANS and quantified by the measurement of the anisotropy factor, which depend on the applied rate, position in the channel and confinement. Further experiments to characterize rheologically the mixture CTAB/NaSal must be done, as well as measurements of the relation times to achieve proper *El* values also for dilute solutions.

## REFERENCES

1. Miller, E. and Rothstein, J. P. (2007), "Transient evolution of shear-banding wormlike micellar solutions", *J. Non-Newtonian Fluid Mech.*, **143**, 22–37.

2. Hofmann, S.; Rauscher, A. and Hoffmann, H. (1991), "Shear induced micellar structures", *Ber. Bunsenges. Phys. Chem.*, **95**, 153-164.

3. Cooper-White, J.J.; Crooks, R.C. and Boger, D.V. (2002), "A drop impact study of worm-like viscoelastic surfactant solutions", *Colloids Surfaces A: Physicochem Eng Aspects,* **210**, 105 – 123.

4. Mohanty, S.; Davis, H.T. and McCormick, A. V. (2001), "Complementary Use of Simulations and Free Energy Models for CTAB/NaSal Systems", *Langmuir*, **17**, 7160-7171.

5. Hartmann, V.; Cressely, R. (1997), "Influence of sodium salicylate on the rheological behaviour of an aqueous CTAB solution", *Colloids Surfaces A: Physicochem Eng Aspects,* **121**, 151-162.

6. Kim, W. J.; Yang, S. M. (2000), "Effects of sodium salicylate on the microstructure of an aqueous micellar solution and its rheological responses", *J. Colloid Interface Sci.,* **232**, 225-234.

7. Hartmann, V. and Cressely, R. (1998), "Occurrence of shear thickening in aqueous micellar solutions of CTAB with some added organic counterions", *Colloid Polym Sci.*, **276**, 169-175.

8. Moss, R.G. and Rothstein, J.P. (2010), "Flow of wormlike micelle solutions past a confined circular cylinder", *J. Non-Newtonian Fluid Mech.*, **165**, 1505-1515

9. Herle, V.; Manneville, S. and Fischer, P. (2008), "Ultrasound velocimetry in a shear-thickening wormlike micellar solution: evidence for the coexistence of radial and vorticity shear bands", *Eur. Phys. J. E*, **26**, 3-12.

10. Wheeler, E.K., Fischer, P. and Fuller, G. G. J. (1998), "Time-periodic flow induced structures and instabilities in a viscoelastic surfactant solution", *Non-Newtonian Fluid Mech.*, **75**, 193 – 208.

11. Vasudevan, M.; Shen, A.; Khomami, B.; Sureshkumar, R. (2007), "Self-similar shear-thickening behavior in CTAB/NaSal surfactant solutions", *Phys. flu-dyn.*, 1-41.

12. Olmsted P.D. (2008), "Perspectives on shear banding in complex fluids", *Rheol. Acta*, **47**, 283-300.

13. Dhont, J.K.G. and Briels, W.J. (2008), "Gradient and vorticity banding", *Rheol. Acta*, **47**, 257-282.

14. Aradian, A. and Cates, M.E. (2006), "Minimal model for chaotic shear banding in shear thickening fluids", *Phys. review E*, **73**, 041508.

15. Herle, V.; Kohlbrecher, J.; Pfister, B.; Fischer,P. and Windhab, E.J. (2007), "Alternating vorticity bands in a solution of wormlike micelles", *Phys. Review Letters*, **99**, 158302.

16. Ezrahi, S.; Tuval, E. and Aserin, A. (2006), "Properties, main applications amd perspectives of worm micelles", *Advances Colloid Interface sci*., **128-130**, 77-102.

17. Rodd, L.E.; Scott, T.P.; Boger, D.V.; Cooper-White, J.J. and McKinley, G.H. (2005), "The inertio-elastic planar entry flow of low-viscosity elastic fluids in microfabricated geometries", *J. Non-Newtonian Fluid Mech.*, **129**, 1–22.

18. Oliveira, M.S.N.; Alves, M.A.; Pinho, F.T. and McKinley, G.H. (2007), "Viscous flow through microfabricated hyperbolic contractions", *Exp. Fluids*, **43**, 437–45.

19. Fischer, P. et al. (2010), PSI experimental report 20070587.

20. Baravian, C. and Quemada, D. (1998), "Using instrumental inertia in controlled stress rheometry", *Rheol Acta,* **37**, 223–233.

21. Schweizer, P.A. (2006), "Corrosion of polymers and elastomers", Taylor & Francis Group, Boca Raton, pp. 108, 121, 451, 518, 530.

22. Tripathi, D. (2002), "Practical Guide to Polypropylene", Rapra Technology Limited, Shawbury, pp. 59-61.

23. Croce, V.; Cosgrove, T.; Dreiss, C.A.; King, S.; Maitland, G. and Hughes, T. (2005), "Giant micellar worms under shear: a rheological study using SANS", *Langmuir*, **21**, 6762-6768.